ELSEVIER

Thermochimica Acta 314 (1998) 55–68

thermochimica acta

A strategy to establish an industrial thermodynamic data bank. The ternary (Pb, Sn, Zn) liquid phase in the zinc purification process. Extension to any quaternary system (M, Pb, Sn, Zn)

J. Hertz, Ch. Naguet, A. Bourkba, J.M. Fiorani, V. Vassiliev, J. Sauvanaud[1,*]

Thermodynamique Métallurgique, Laboratoire de Chimie du Solide Minéral-URA CNRS 158, Université Henri Poincaré, Nancy I, B.P. 239-54506, Vandoeuvre lès Nancy Cedex, France

Received 4 August 1997; accepted 3 November 1997

Abstract

In the zinc thermal process, the separation of lead can be achieved using the liquid miscibility gap in the Pb–Zn system. Various impurities can be simultaneously extracted in the lead phase depending on the mutual solubilities, well-characterised by the tie-lines inside the multicomponent miscibility gap. This paper will describe the strategy needed to establish a thermodynamic (M, Pb, Sn, Zn) data bank suitable to accurately calculate this particular phase diagram: a miscibility gap is especially difficult to fit because its shape is strongly related not only to the Gibbs function and its first derivatives but also to its second-order derivatives. A systematic exploitation of the literature was insufficient to realise this goal, and calorimetric measurements in the multicomponent system were needed to model the enthalpy contribution; the entropy contribution was determined by emf experiments using sealed cells and a molten-salt mixture electrolyte. Finally, a Thermo-Calc optimisation was used to fit together all the superabundant information. This strategy will be described in some detail and illustrated by some graphical results concerning our experiments and the calculated (Pb, Sn, Zn) miscibility gap, in spite of the fact that the data bank will remain unpublished as an industrial property. © 1998 Elsevier Science B.V.

Keywords: Liquid miscibility gap; Multicomponent alloys; Pb, Sn, Zn; Phase diagram; Zinc process

1. Introduction

The use of a miscibility gap in the liquid phase is a convenient way to refine lead–zinc based alloys. According to the Massalski et al. [1], the zinc boundary in the binary (Pb, Zn) phase diagram at a temperature close to 450°C is very near to pure zinc (Fig. 10). Melting the alloy at this temperature the liquid phase separates into two phases: at the top of the furnace a liquid zinc phase and at the bottom a lead-rich liquid phase. Since, the densities of these two phases are very different a partition occurs which allows extracting nearly pure zinc.

Obviously, there still exist impurities like tin and others that may strongly change the peculiarities of the binary miscibility gap. To know the effects of each impurity we have to perform a thermodynamic assessment of the *n*-ary liquid phase (where *n* is the number of components) using reliable experimental data. With such a work we can forecast the influence of any one

*Corresponding author.

[1]Metaleurop-Recherche: 1 avenue Albert Einstein, B.P. 120, F-78193 Trappes Cedex, France.

PII S0040-6031(97)00456-5

impurity in the presence of all the others and calculate all the thermochemical quantities such as the tie-lines in the multicomponent miscibility gap or the activities of these different components.

2. Generalities concerning the miscibility gap calculation

A miscibility gap is a special case of phase equilibrium in which one phase of the system becomes thermodynamically unstable in a certain range of compositions. The locus where the chemical stability is destroyed is called the spinodal locus. In a binary system, this spinodal locus is a curve in the (T, x_2), axis diagram. The spinodal condition in a binary system is $(\partial\mu_1/\partial x_1)_{p,T}=0$ or $(\partial\mu_2/\partial x_2)^{p,T}=0$, where μ_i is the chemical potential and x_i the mole fraction. These two conditions are equivalent in a binary system. In a ternary system, the 'spinodal locus' is a surface in the (T, x_1, x_2) axis diagram. In a quaternary solution, the 'spinodal locus' is a hypersurface of dimension three in the (T, x_1, x_2, x_3) axis diagram and so on.

When any phase becomes unstable this phase separates into two parts where each is in equilibrium with the second one. The isothermal segments linking the equilibrium compositions of the two coexistent phases are called the tie-lines. In the phase diagram, the extremities of all the tie-lines describe the 'binodal surface.' The binodal and the spinodal surfaces have the same dimension in the (T, x_i) space, equal to the number of components present in the system.

In a binary system an equilibrium between two phases corresponds to the existence of a common tangent linking two separate Gibbs functions (Fig. 1). Each Gibbs function is relative to one phase and exhibits a complete convexity. The common tangent minimizes the mean Gibbs function.

On the contrary, a miscibility gap appears when the Gibbs function of one sole phase exhibits a change of convexity (spinodal conditions). In such a case there exists a common tangent between two different points of the same Gibbs function belonging to this sole phase (Fig. 2). The change of convexity of the Gibbs function is linked to its second-order derivatives vs. the mole fractions. For this reason such a phase diagram optimisation needs a very accurate mathematical representation of the Gibbs function up to its second-order derivatives, well consistent with physical reality. The spinodal locus is always included inside the binodal locus as appears in Fig. 2.

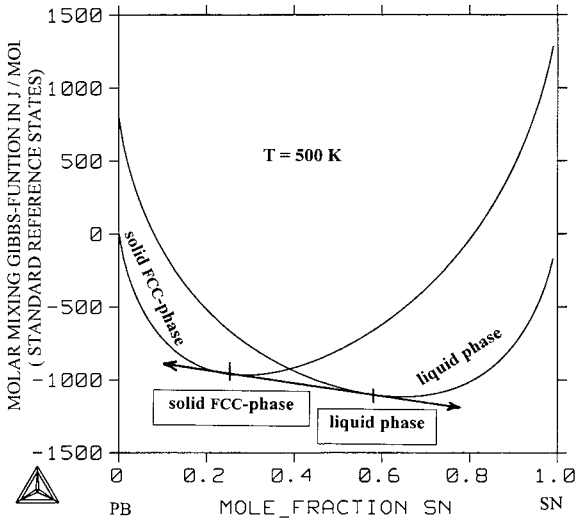

Fig. 1. An example of thermodynamic equilibrium between two different phases: representation of the Gibbs functions at 500 K for the FCC lead-rich phase and the liquid tin-rich phase in the (Pb, Sn) binary system. The tie-line (or binodal-segment) links the two curves by a common tangent which minimises the mean Gibbs function in the biphase domain.

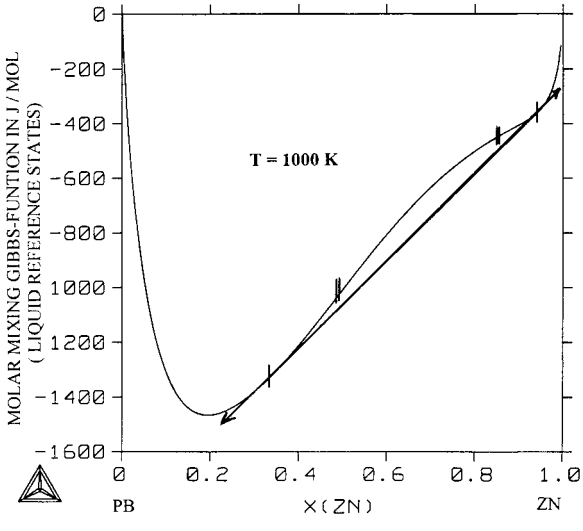

Fig. 2. An example of thermodynamic equilibrium between two different compositions of the same phase: the Gibbs function of the liquid binary (Pb, Zn) phase calculated at 1000 K. The unstable compositions of the liquid phase are included between the two spinodal inflexion points (II), whereas the tie-line or binodal segment links the two contacts (I) with the common tangent.

3. The Thermo-Calc optimisation of the multicomponent systems

The most useful manner to represent mathematically the molar Gibbs function of a solution φ is to decompose it into three terms:

$$G_{\mathrm{m}}^{\varphi}(p,T,x_i) = \sum_{i=1}^{i=c} x_i^{\varphi}\mu_i^*(p,T) + RT\sum_{i=1}^{i=c} x_i^{\varphi}\ln x_i^{\varphi} + G_{\mathrm{m}}^{\mathrm{E}}. \quad (1)$$

The first term in the second member of Eq. (1) is called the reference term and represents the mean value of the Gibbs function of all the pure components μ_i^*, each one taken in its right mole fractions x_i^{φ} in the phase φ.

In a coherent thermodynamic data bank, the reference terms in Eq. (1) are described for each component. The Scientific Group Thermodata Europe (SGTE) has established a coherent data bank of pure metals well suitable for alloy phase diagram optimisation and implemented in the Thermo-Calc software developed by Sundman et al. [3]. This program was managed by Mats Hillert (starting in the seventies, with the big development of computers), in the Royal Institute of Technology of Stockholm (KTH). The Thermo-Calc program is still evolving continuously, providing more and more possibilities.

The second term of Eq. (1) is called the ideal mixing term and corresponds to the entropy contribution of an ideally disordered mixture of species, in a substitution solution.

The third term $G_{\mathrm{m}}^{\mathrm{E}}$ is the excess Gibbs molar function and is, generally, modeled by a polynomial function vs. the mole fractions x_i^{φ}, and often by a linear extension vs. T, corresponding to the decomposition of $G_{\mathrm{m}}^{\mathrm{E}}$ into the molar enthalpy of mixing H_{m} and the excess molar entropy of mixing $S_{\mathrm{m}}^{\mathrm{E}}$:

$$G_{\mathrm{m}}^{\mathrm{E}} = H_{\mathrm{m}} - TS_{\mathrm{m}}^{\mathrm{E}}. \quad (2)$$

Using the so-called Gibbs–Duhem equation each term in Eq. (2) can be described as a linear extension of the mole fractions, (also called the Euler equations).

$$G_{\mathrm{m}}^{\mathrm{E}} = \sum_{i=1}^{i=c} x_i^{\varphi}\mu_i^{\mathrm{E}} \quad (3)$$

where μ_i^{E} are the excess chemical potentials

$$H_{\mathrm{m}} = \sum_{i=1}^{i=c} x_i^{\varphi}\overline{H}_i \quad (4)$$

where $\overline{H}_i$ are the partial enthalpies of mixing

$$S_{\mathrm{m}}^{\mathrm{E}} = \sum_{i=1}^{i=c} x_i^{\varphi}\overline{S}_i^{\mathrm{E}} \quad (5)$$

where $\overline{S}_i^{E}$ are the excess entropies of mixing

$$\mu_i^{\mathrm{E}} = \overline{H}_i - T\overline{S}_i. \quad (6)$$

The integral enthalpy of mixing H_{m} and the partial molar enthalpy of mixing $\overline{H}_i$ can be measured directly by calorimetry: the integral enthalpy of mixing is the total heat evolving during the mixture formation, whereas the partial molar enthalpy represents the heat derivative vs. one mole of component i in the mixture. On the contrary, the entropy contribution cannot be measured directly. Only the chemical excess potential μ_i^{E}, as in Eq. (6) can be measured by emf experiments.

For these reasons two different types of experiments are required to obtain the Gibbs function of any phase: calorimetric measurements to obtain the mixing enthalpy and emf measurements for the chemical potential, including the entropy contribution.

The most convenient way to represent the excess Gibbs function $G_{\mathrm{m}}^{\mathrm{E}}$ vs. composition in a multicomponent phase is the Redlich–Kister polynomial extension [4]

$$G_{\mathrm{m}}^{\mathrm{E}} = \sum_{i,j} x_i x_j \sum_{n=0}^{n} a_n^{ij}(x_i - x_j)^n + \sum_{i,j,k} x_i x_j x_k (A_i^{ijk}V_i + A_j^{ijk}V_j + A_k^{ijk}V_k). \quad (7)$$

In Eq. (7) the a_n^{ij} coefficients are exactly those of the binary border alloys, but we have to underline that in a multicomponent phase $x_i+x_j\neq 1$, which means that these 'binary contributions' are taken at the orthogonal projections of the composition of the phase on the binary axis.

The V_i coordinates have been proposed by Hillert [5]

$$V_i = x_i + \frac{1-(x_1+x_2+x_3)}{3}, \quad (8)$$

in a ternary system $V_i=x_i$.

Taking into account Eq. (2) each a_n^{ij} and A_i^{ijk} adjustable coefficient has an enthalpy and an entropy contribution.

The Thermo-Calc software is organised with different modules, each one devoted to a particular function. The more important modules are TDB, PARROT and POLY each of which is linked to the others.

The PARROT module is the optimisation module. All the experimental information, like the mixing enthalpies, the chemical potentials, the compositions of the tie-lines in the phase diagram can be introduced in the PARROT module. The function of PARROT is to calculate the a_n^{ij} and A_i^{ijk} adjustable coefficients which optimise all this over-abundant experimental data series.

The POLY module is devoted to the calculation of any phase diagram in a two-dimensional mapping. This means that only two variables are allowed to vary simultaneously in this representation. Also, any variable like μ_i, G_m^E, H_m, S_m^E, x_i^{φ} ... can be calculated and plotted in a two-dimensional representation.

The TDB module is devoted to the storage of the thermodynamic data bank. It collects all the adjusted and SGTE parameters in the same file on a very concentrated place-memory for the computer disk. As a comparison a PARROT-file needs several Mos in the central disk, whereas the same information for the POLY module can be provided by a TDB-file using only a few kos.

The Thermo-Calc software itself includes different data banks corresponding to the already optimised systems. In particular many binary metallic systems are now coherently available in the data banks. But any user of Thermo-Calc can also build its own data bank including the data for its particular needs. This is clear for the multicomponent systems because only a few are available in any international data bank.

4. The (literature+experiments) strategy

4.1. Literature discrepancy

In view of obtaining a precise representation for the ternary (Pb, Sn, Zn) liquid miscibility gap and also for other quaternary (M, Pb, Sn, Zn) systems, we have first collected in the literature all the available data concerning the binary sub-systems. By introducing all these data in the Thermo-Calc software it, unfortunately, appeared that no coherent answer can be obtained based on the literature. The principal physical reason for the existence of a miscibility gap in the (Pb, Zn) system is the strong endothermic mixing enthalpy. Unfortunately this mixing enthalpy is very difficult to obtain by calorimetry: at low temperatures the system is unmixed and at high temperatures the vapor pressure of zinc is so high that zinc flows out of the crucible by vaporisation. Fig. 3 shows different contradictory results of this binary mixing enthalpy collected in the literature. The discrepancy between the different sources is more than 50% of the higher one.

4.2. Experiments

Since experimental data published in the literature were not sufficient to make our assessment, we have performed calorimetric and emf measurements in view of obtaining independently the mixing enthalpy and the zinc activity for several compositions.

4.2.1. Calorimetric measurements

The mixing enthalpy measurements in the liquid monophase were performed in a Calvet-type calorimeter, using a drop method [6–8]. However, in some cases this method cannot be applied for several reasons. For instance, in the (Pb, Zn) system the large miscibility gap and the high volatility of zinc prevent this kind of measurement. To solve this problem, Todd and Oates [9] have used the heat content of (Pb, Zn) alloys measured by drop calorimetry between 900°C and room temperature: the liquid phase at high temperature is in a homogeneous phase, whereas at room temperature the components separate into the two pure solid components, for this reason the heat content measurement includes the mixing enthalpy. We have used another strategy to measure the (Pb, Zn) mixing enthalpy [7]. In a ternary (M, Pb, Zn) phase diagram the liquid homogeneous phase exists at a low temperature (720 K) outside the miscibility gap. By measuring the mixing enthalpy in this ternary system, it was possible to establish its Redlich–Kister ternary representation and to extrapolate this equation to the binary (Pb, Zn) border, where the liquid phase is unstable.

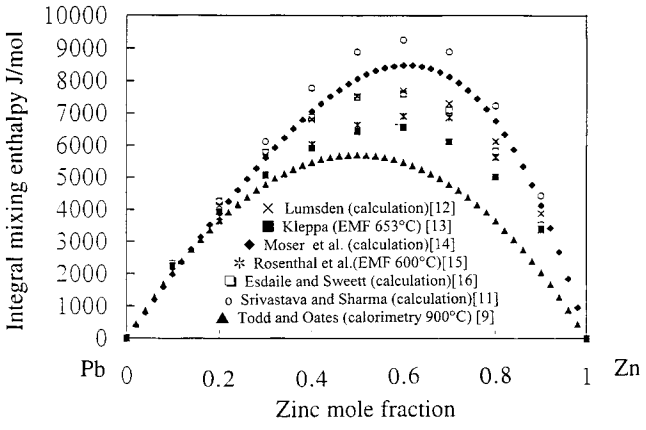

Fig. 3. Illustration of the discrepancy of the literature data concerning the mixing enthalpy of the binary (Pb, Zn) liquid phase: all these values have been proposed by different authors in the 600–900°C range.

This strategy was successful and the results obtained with the (Pb, Sn, Zn) and other (M, Pb, Zn) ternary systems gave very coherent data, also in good agreement with Todd and Oates results.

With the (Pb, Sn, Zn) extrapolation we got:

$$H_m(\mathrm{Pb,Zn}) = x_{\mathrm{Pb}}x_{\mathrm{Zn}}[23042 - 3603(x_{\mathrm{Pb}} - x_{\mathrm{Zn}}) + 1465(x_{\mathrm{Pb}} - x_{\mathrm{Zn}})^2] \quad (9)$$

and with the (M, Sn, Zn) system.

$$H_m(\mathrm{Pb,Zn}) = x_{\mathrm{Pb}}x_{\mathrm{Zn}}[22912 - 2805(x_{\mathrm{Pb}} - x_{\mathrm{Zn}}) + 354(x_{\mathrm{Pb}} - x_{\mathrm{Zn}})^2]. \quad (10)$$

Fig. 4 shows the graphical plot of the two relations (9) and (10) together with the regular model proposed by Todd and Oates [9]. The discrepancy between the values calculated by Eqs. (9) and (10) does not exceed 160 J/mol.

For the (Pb, Sn, Zn) ternary liquid phase, we obtained the integral mixing enthalpy values presented in Table 1. Details of this study have been already described in [6].

For the quaternary (M, Pb, Sn, Zn) system where M is another metal, we have performed calorimetric measurements following various binary, ternary, then quaternary paths. Fig. 5 summarises these paths in the quaternary composition tetrahedron. Each one starts from one pure component apex, then goes to the middle of a binary edge, then to the center of a ternary face and finally to the center of the quaternary composition tetrahedron. All these paths have been chosen outside the quaternary miscibility gap. In such a procedure the center of the tetrahedron has been attained three times, providing a control of the consistency of the experimental measurements and an estimation of the uncertainty: ±100 J/mol at the center of the tetrahedron.

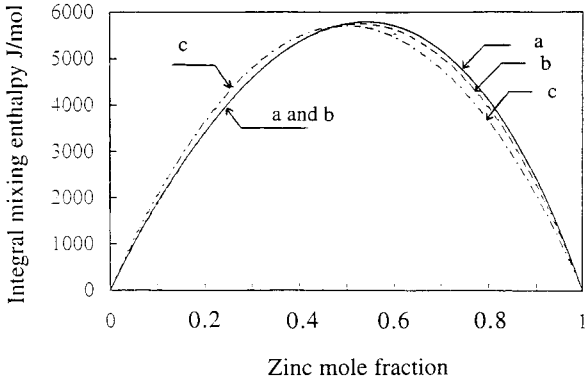

Fig. 4. (a) Continuous line: the (Pb, Zn) mixing enthalpy obtained by extrapolation (up to the binary Pb–Zn border) of the ternary Redlich–Kister (Pb, Sn, Zn) mixing enthalpy equation. The experimental data have been measured outside the ternary miscibility gap; (b) Dashed line: the same method applied to another ternary (M, Pb, Zn) system; and (c) Point-dashed line: comparison with the regular solution model proposed by Todd and Oates [9] according to their heat content experiments.

Table 1
The integral mixing enthalpy H_m (Pb, Sn, Zn) measured at 717 K

x_{Pb} (mol%)	x_{Sn} (mol%)	x_{Zn} (mol%)	H_m (J/mol)
Isopleth $x_{Pb}=x_{Sn}$			
48.5	48.5	3	1895
47	47	6	2256
45.5	45.5	9	2604
44	44	12	2920
42.5	42.5	15	3121
41	41	18	3506
39.5	39.5	21	3755
38	38	24	3982
36.5	36.5	27	4188
35	35	30	4354
33.34	33.34	33.32	4506
Isopleth $x_{Sn}=x_{Zn}$			
3	48.5	48.5	3601
6	47	47	3793
9	45.5	45.5	3963
12	44	44	4088
15	42.5	42.5	4185
18	41	41	4271
21	39.5	39.5	4330
24	38	38	4360
27	36.5	36.5	4361
30	35	35	4346
33.33	33.33	33.33	4311
Isopleth $2x_{Pb}=3x_{Sn}$			
58.8	39.2	2	1786
57.6	38.4	4	2051
56.18	37.45	6.37	2355
55.2	36.8	8	2560
54	36	10	2798
52.8	35.2	12	3017
51.6	34.4	14	3223
50.4	33.6	16	3425
49.2	32.8	18	3610
48	32	20	3783
46.8	31.2	22	3947
45.6	30.4	24	4085
44.4	29.6	26	4205

4.2.2. emf measurements

Using a concentration cell with a molten-salt mixture electrolyte, we measured the zinc activity in ternary and quaternary systems inside and outside the miscibility gap, thus also providing some experimental points of the binodal surface. Basically, such a cell is composed of one pure zinc anode and one cathode made with an alloy containing zinc. The emf

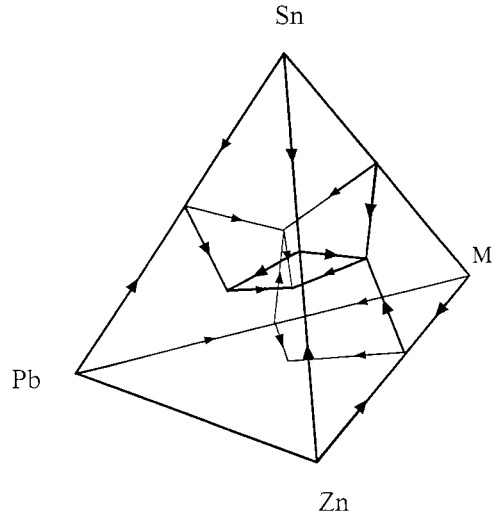

Fig. 5. The various composition – paths used to obtain the quaternary mixing enthalpy up to the center of the tetrahedron. All these paths have been chosen outside the miscibility gap. Each individual series starts at one component apex, then joins the middle of a binary edge, then the center of a ternary face and finally the center of the quaternary tetrahedron.

signal between the two electrodes, E, is measured at a fixed temperature, T. Then varying step by step, the temperature T, we may obtain the $E(T)$ curve as in Fig. 6. The Nernst law gives the relation between E, T and the zinc activity in the alloy a_{Zn}:

$$a_{Zn} = \exp\left(\frac{-2FE}{RT}\right). \quad (11)$$

F and R are the Faraday and the perfect-gas constants, respectively.

Each cell-device allowed us to study simultaneously seven different electrodes: we used two pure zinc anodes to verify the zero answer, and the five other electrodes were devoted to various alloy compositions. In the ternary (Pb, Sn, Zn) system, we have chosen five compositions (shown in Fig. 7) in view of crossing the binodal surface with each alloy in our experimental range between 400 and 550°C.

Table 2 presents the results of our emf study obtained with these five (Pb, Sn, Zn) alloys: the equilibrium state of the alloys vs. temperature, the $E(T)$ linear fit for each composition inside and outside the miscibility gap as well as the binodal temperature boundary and the experimental points selected for our Thermo-Calc optimisation.

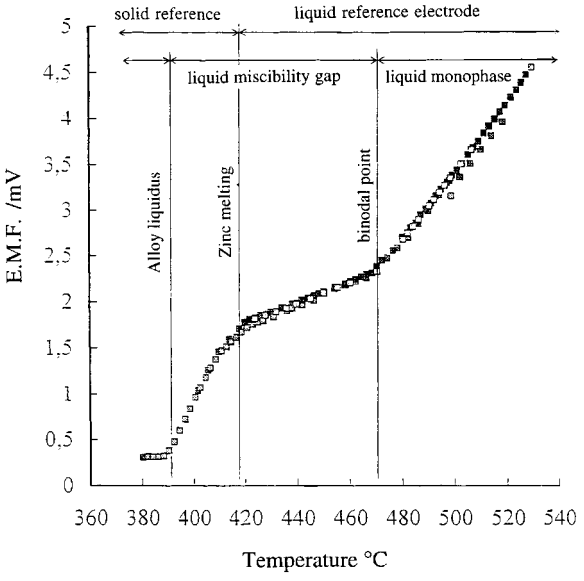

Fig. 6. A typical emf $E(T)$ curve showing four different steps: starting from high temperatures and going to low temperatures we observe a straight line in the monophase liquid phase, a straight line in the miscibility gap, a straight line between the melting point of the reference electrode (419.5°C) and the liquidus of the alloy electrode, a short segment in the mixed solid–liquid domain for the alloy-electrode.

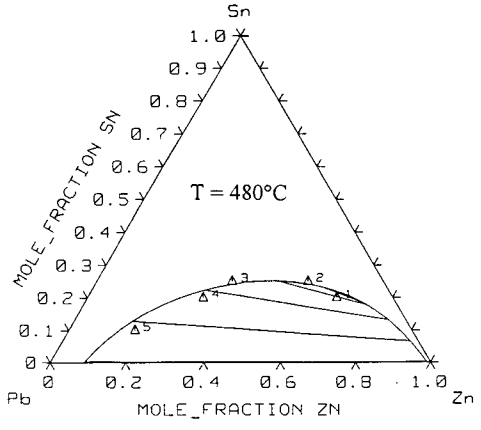

Fig. 7. The experimental alloy compositions chosen to study the (Pb, Sn, Zn) miscibility gap. These five alloys have been designed to cross the binodal surface in the range of our emf experimental temperatures. The curve is the miscibility gap at 480°C optimized in the present work.

4.2.2.1. Other ternary and quaternary alloys. Using exactly the same emf method other ternary (M, Pb, Zn) or quaternary (M, Sn, Pb, Zn) alloys have been studied giving a sufficient set of data for the final quaternary Thermo-Calc optimisation. Two orthogonal quaternary isoplethic cuts have been explored by emf with the following conditions: $x_{Sn}=x_M$ and $x_{Pb}=x_{Zn}$ as drawn in Fig. 8.

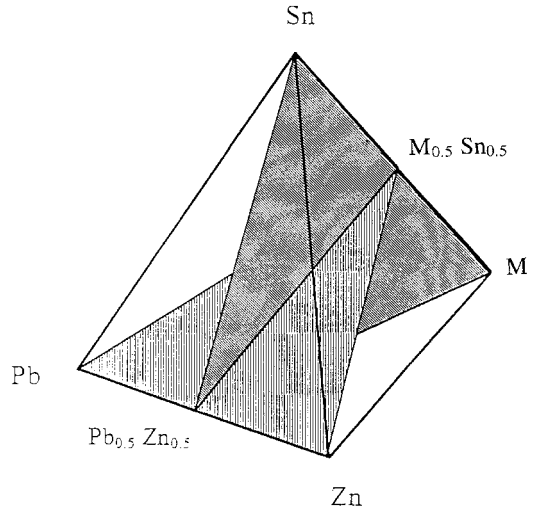

Fig. 8. The two orthogonal quaternary isopleths used to explore the quaternary miscibility gap by emf: the goal was to obtain a maximum information with a minimum set of experiments.

5. The Thermo-Calc optimisation

5.1. Introducing the data in the PARROT module

The optimisation of the (M, Pb, Sn, Zn) quaternary system is done stepwise. At first we optimise the six binary sub-systems, then the four ternary sub-systems and, finally, the quaternary one. At each step an over-abundant set of data is established and compiled in the Parrot module. All the experimental series include the literature data, like phase diagram boundaries, mixing enthalpies or activities as well as our own experimental data especially devoted in order to complete the literature: the ternary and quaternary mixing enthalpies, the emf ternary and quaternary zinc activities, the binodal boundaries for miscibility gap in the ternary and quaternary systems. Our own explored literature included more than 80 references and the experimental work for calorimetry and emf measurements

Table 2
emf experimental results in the (Pb, Sn, Zn) system: selected values for the optimisation

Alloy composition	Temperature range (°C)	Equilibrium state	Temperature (°C)	emf (mV)	Zinc activity	emf linear variation $E(\text{mV})=a+bt(^\circ\text{C})$	ΔE(mV) uncertainty
			440	2.619	0.918		
$Pb_{0.150}$ $Sn_{0.200}$	419.5–505.2	Biphase	460	2.861	0.913	$a=-2.70\pm0.08$	0.02
$Zn_{0.650}$	binodal 505.2°C		*480*	*3.103*	*0.909*	$b=(12.09\pm0.16)\times10^{-3}$	
nr 1	505.2–552		515	3.648	0.898		
		Monophase	535	4.138	0.888	$a=-8.99\pm0.60$	0.06
			550	4.506	0.881	$b=(24.50\pm1.09)\times10^{-3}$	
			430	2.556	0.919		
$Pb_{0.200}$ $Sn_{0.250}$	419.5–467.3	Biphase	440	2.706	0.916	$a=-3.88\pm0.25$	0.02
$Zn_{0.550}$	binodal 467.3°C		*460*	*3.005*	*0.909*	$b=(14.97\pm0.57)\times10^{-3}$	
nr 2			480	3.502	0.989		
	467.3–547		500	4.111	0.884	$a=-11.13\pm0.24$	0.06
		Monophase	520	4.721	0.871	$b=(30.48\pm0.49)\times10^{-3}$	
			540	5.331	0.859		
			430	2.381	0.924		
$Pb_{0.400}$ $Sn_{0.250}$	419.5–472.4	Biphase	440	2.575	0.920	$a=-5.93\pm0.45$	0.06
$Zn_{0.350}$	binodal 472.4°C		*460*	*2.961*	*0.910*	$b=(19.30\pm1.03)\times10^{-3}$	
nr 3			480	3.720	0.892		
	472.4–528		500	5.088	0.858	$a=-29.11\pm0.94$	
		Monophase	520	6.456	0.829	$b=(68.40\pm1.94)\times10^{-3}$	0.14
			440	2.360	0.926		
$Pb_{0.500}$ $Sn_{0.200}$	419.5–505.9	Biphase	460	2.616	0.920	$a=-3.28\pm0.13$	0.04
$Zn_{0.300}$	binodal 505.9		480	2.872	0.915	$b=(12.81\pm0.26)\times10^{-3}$	
nr 4	505.9–548		*500*	*3.129*	*0.910*		
			515	3.709	0.896	$a=-24.79\pm0.72$	0.06
			535	4.815	0.871	$b=(55.30\pm1.40)\times10^{-3}$	
		Monophase	550	5.645	0.853		
			440	1.893	0.940		
$Pb_{0.725}$ $Sn_{0.100}$	419.5–521.1	Biphase	460	2.113	0.935	$a=-2.96\pm0.31$	0.10
$Zn_{0.175}$			480	2.334	0.931	$b=(11.03\pm0.65)\times10^{-3}$	
nr 5	binodal 521.1		*500*	*2.555*	*0.926*		
			530	3.498	0.904		
	521.1–548	Monophase	540	4.296	0.885	$a=-38.80\pm4.70$	0.08
			550	5.095	0.866	$b=(79.80\pm8.68)\times10^{-3}$	

comprised theses by two students over a period of three years.

5.2. *The results obtained in the (Pb, Sn, Zn) ternary system using the Thermo-Calc TDB module*

This particular ternary system allowed us to give a good example of our final optimisation and to compare the calculated phase diagram with the literature. This ternary system includes four different phases: the liquid phase which decomposes in the miscibility gap; the lead isomorphic FCC-A1 primary solution; the tin isomorphic BCT-A5 primary solution; and the zinc isomorphic HCP-A3 primary solution.

In our data bank the final optimised equations for the excess Gibbs functions are the following, the thermodynamic properties of the stable pure elements are those of the SGTE international data bank [2].

Liquid phase, with the pure liquid Pb, Sn, Zn as reference states:

$$G_m^E(\text{liquid}) = x_{Pb}x_{Sn}[6004 - 0.5294T + 107(x_{Pb} - x_{Sn})] + x_{Pb}x_{Zn}[22997 - 3.98T - (3866 + 0.3128T)(x_{Pb} - x_{Zn}) + 2334(x_{Pb} - x_{Zn})^2 - 1.1564T(x_{Pb} - x_{Zn})^3 - 3.3031T(x_{Pb} - x_{Zn})^5] + x_{Sn}x_{Zn}[12592 - 8.723T - (5064 - 3.1647T)(x_{Sn} - x_{Zn}) + (2893 - 1.941T)(x_{Sn} - x_{Zn})^2] - x_{Pb}x_{Sn}x_{Zn}[1390 + (3.951x_{Pb} - 6.071x_{Sn} + 18.067x_{Zn})T]. \quad (12)$$

Lead primary solution with Pb-FCC, Sn-BCT, Zn-HCP as reference states:

$$G_m^E(\text{FCC}) = x_{Pb}x_{Sn}(8590 - 6.43T) + x_{Pb}x_{Zn}(30000 - 17.16T) + x_{Sn}x_{Zn}13000 + x_{Sn}(4150 - 5.2T) + x_{Zn}(2281 - 1.694T). \quad (13)$$

Tin primary solution with Pb-FCC, Sn-BCT, Zn-HCP as reference states:

$$G_m^E(\text{BCT}) = x_{Pb}x_{Sn}12049 + x_{Pb}x_{Zn}23000 + x_{Sn}x_{Zn}29.90T + x_{Pb}(489 + 3.52T) + x_{Zn}6077. \quad (14)$$

Zinc primary solution with Pb-FCC, Sn-BCT, Zn-HCP

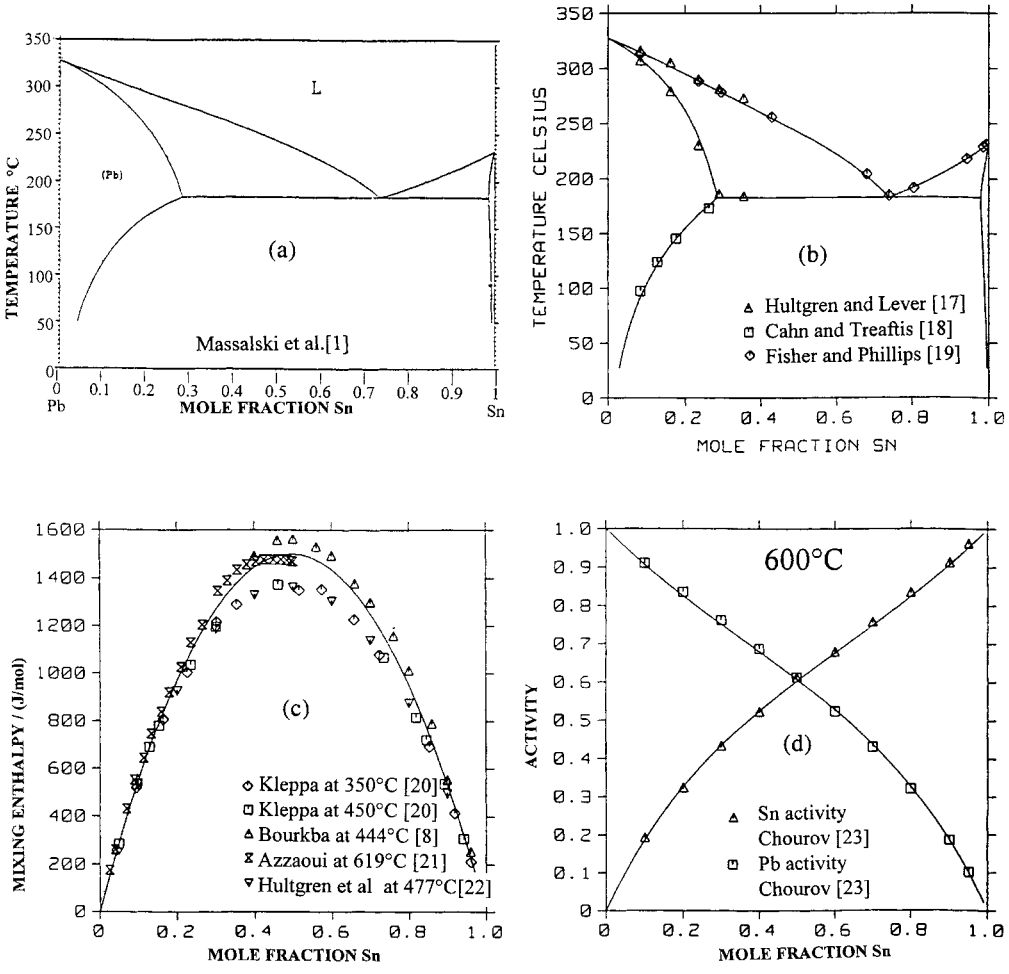

Fig. 9. Optimisation of the (Pb, Sn) system: (a) the literature phase diagram [1]; (b) the calculated phase diagram together with some experimental data points; (c) the mixing enthalpy curve calculated at 500°C, together with some experimental data points; and (d) the tin and lead activities calculated at 600°C together with the experimental points of Chourov [12].

as reference states:

$$G_m^E(\mathrm{HCP}) = x_{Pb}x_{Sn}7000 + x_{Pb}x_{Zn}44893 + x_{Sn}x_{Zn}20998 + x_{Pb}(300 + T) + x_{Sn}(3900 - 4.4T). \quad (15)$$

5.3. Some diagrams obtained with the Thermo-Calc Poly module and our data bank

Figs. 9–11 show the three binary borders of the (Pb, Sn, Zn) system: Fig. 9(a), Fig. 10(a) and Fig. 11(a) show the literature phase diagrams as accepted by Massalski et al. [1], Fig. 9(b), Fig. 10(b) and Fig. 11(b) show our own calculated phase diagrams obtained with our data bank. Some liquidus and solidus experiments are typed in these Fig. 9(b), Fig. 10(b) and Fig. 11(b). The Fig. 9(c), Fig. 10(c) and Fig. 11(c) curves are the mixing enthalpies with the liquid components as reference states, and calculated with our data bank. Some experimental points are typed simultaneously. The Fig. 9(d), Fig. 10(d) and Fig. 11(d) curves are some zinc-activity curves,

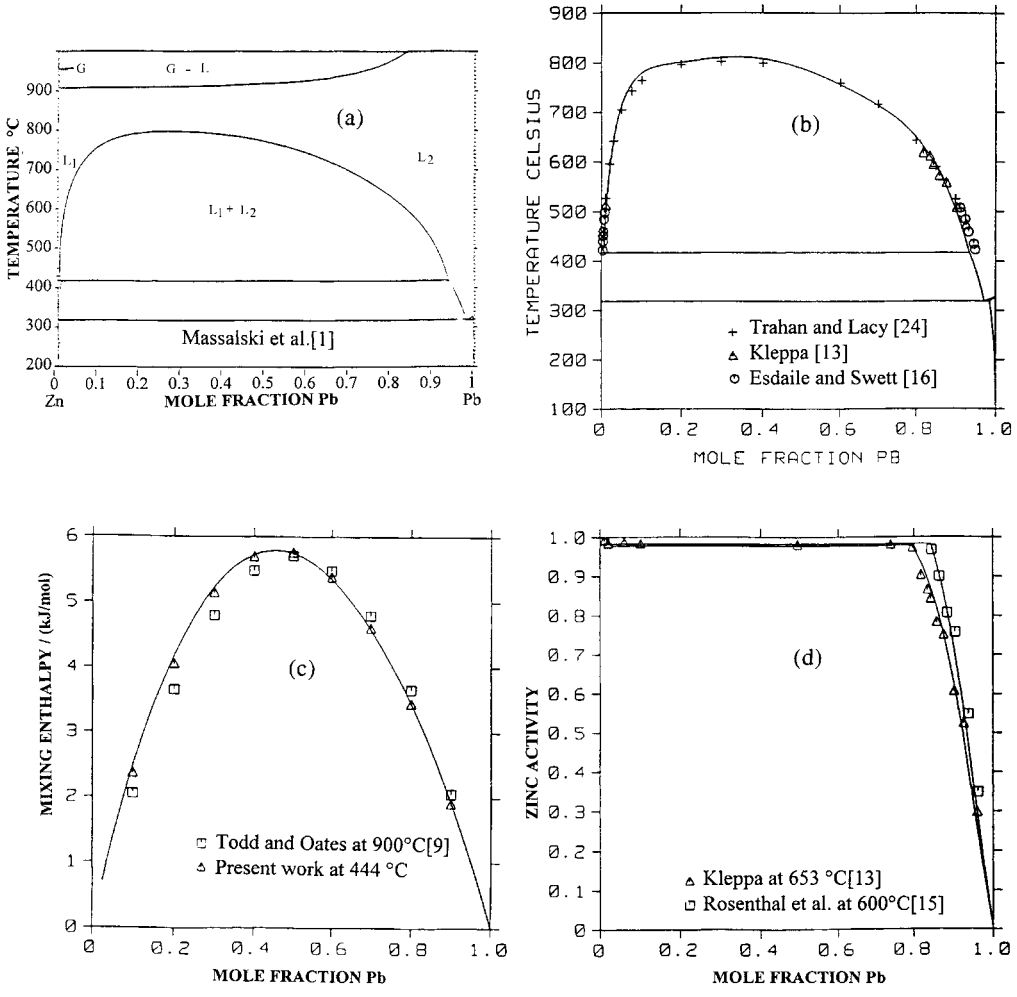

Fig. 10. Optimisation of the (Pb, Zn) system: (a) the literature phase diagram [1]; (b) the calculated phase diagram together with some experimental points; (c) the mixing enthalpy curve calculated at 500°C in the monophase liquid together with our extrapolated experimental points (Fig. 5) and the values of Todd and Oates [9]; and (d) the equilibrium zinc-activity curves at two temperatures and comparison with the literature.

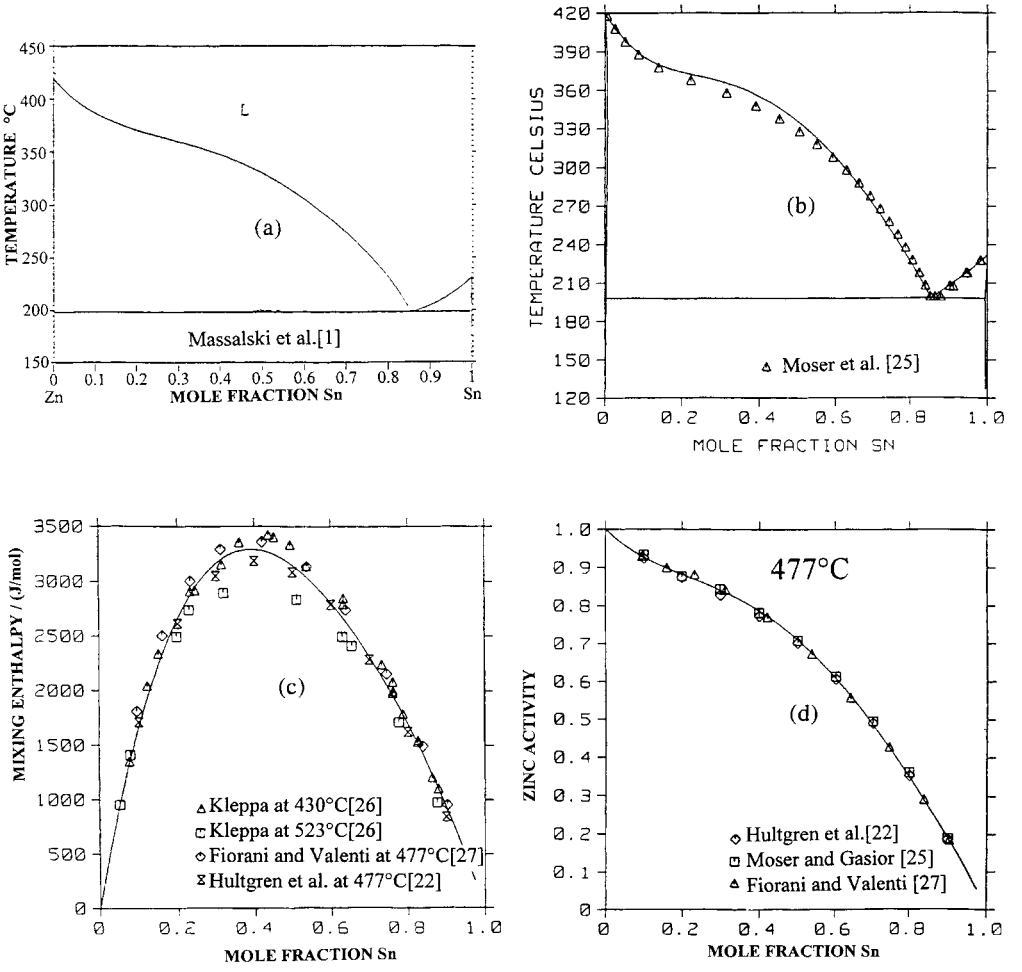

Fig. 11. Optimisation of the (Sn, Zn) system: (a) the literature phase diagram [1]; (b) our calculated phase diagram together with a literature experimental liquidus; (c) the mixing enthalpy calculated at 500 K with some literature data; and; (d) the zinc activity curve calculated at 477°C with some experimental data taken from the literature.

calculated at different temperatures with our data bank and compared with some experimental data points. The consistency with the literature is valid for the phase diagrams, as well as for the mixing enthalpies (±150 J/mol) and the zinc activities (±1%).

Figs. 12 and 13 are a comparison between the ternary (Pb, Sn, Zn) miscibility gap at 700 and 450°C calculated with our own data bank or proposed in the experimental work of Fiorani and Oleari [10]: it is clear from these two figures that the miscibility gap obtained by us is much smaller than that in the literature data. The same observation can be made for the recent calculation of Srivastava and Sharma [11]. Nevertheless, our optimisation is in very good agreement with our own experimental binodal points as presented in Fig. 7 and in Table 2. The zinc activity measurements of Fiorani and Oleari [10] realised in the three isoplethic cuts 3 $x_{Pb}=x_{Sn}$, $x_{Pb}=x_{Sn}$ and $x_{Pb}=3$ x_{Sn} are also in excellent agreement with our model (Figs. 14–16).

5.4. The quaternary (M, Pb, Sn, Zn) miscibility gap representation

For a quaternary system, it is difficult to represent in a two-dimensional plot the miscibility gap with its

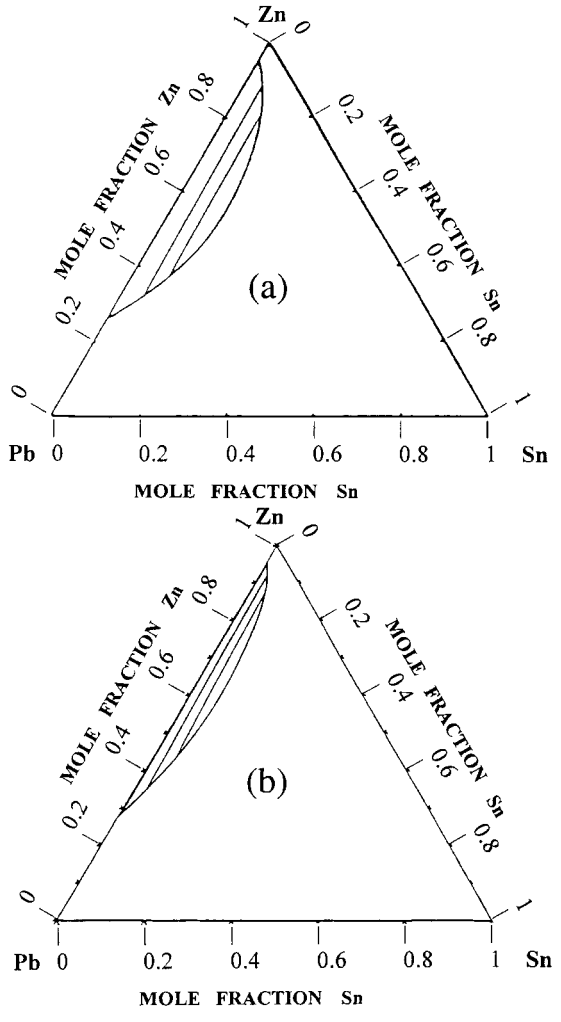

Fig. 12. The (Pb, Sn, Zn) miscibility gap at 700°C: (a) the proposal of Fiorani and Oleari [10] and; (b) our own calculation. The literature miscibility gap appears too large in comparison with the present work.

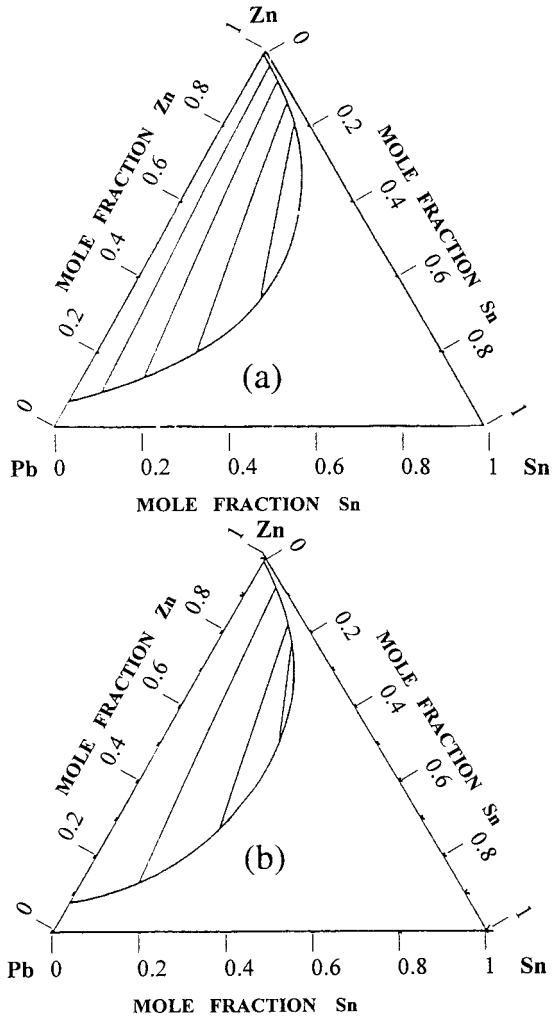

Fig. 13. The (Pb, Sn, Zn) miscibility gap at 450°C, comparison with the literature proposal: (a) the Fiorani and Oleari micibility gap [10]; (b) the present work well consistent with our own experiments: our data provide a smaller surface for the miscibility gap and also a more important rotation of the tie-lines when increasing the Sn content inside the gap.

tie-lines. Nevertheless, considering that on each tie line the four components have a fixed activity it is useful to cut the quaternary phase diagram by such surfaces where the temperature and one activity for one component are simultaneously fixed. Fig. 17 is an example of a particular (M, Pb, Sn, Zn) quaternary system introduced in our data bank. The four phase diagrams presented in this Fig. 17 with the tie-lines have been calculated at the same temperature, with the M activities 10^{-10}, 5×10^{-2}, 10^{-1} and 1.5×10^{-1}.

6. Conclusion

In order to obtain an accurate thermodynamic data bank well suited for providing good provisions in an industrial process, it is necessary to use a particular strategy where new experimental studies are undertaken in overcoming the deficiencies to complete the literature compilation. These new experiments have to be chosen with the aim of bringing together the

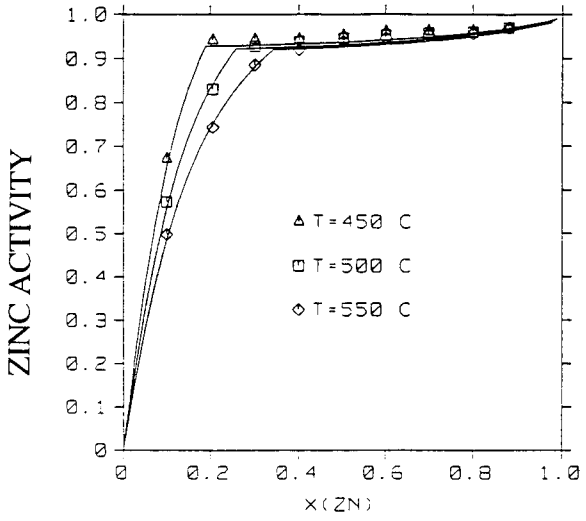

Fig. 14. The zinc activity measurements of Fiorani and Oleari [10] in the isoplethic cut 3 $x_{Sn}=x_{Pb}$ are in excellent agreement with our modelisation: three calculated curves at 450, 500 and 550°C.

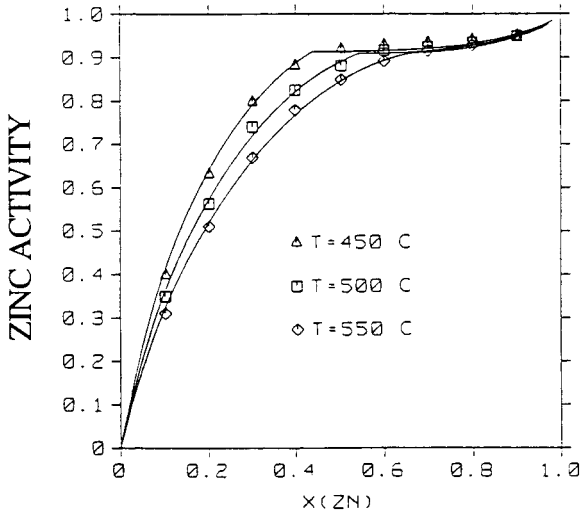

Fig. 15. The zinc-activity measurements of Fiorani and Oleari [10] in the isoplethic cut $x_{Sn}=x_{Pb}$ are in excellent agreement with our modelisation: three calculated curves at 450, 500 and 550°C.

minimum set of phase diagram and thermodynamic information on the whole, lacking in the literature data.

The Thermo-Calc software available at the Royal Institute of Technology of Stockholm is still a very flexible tool well-designed to build its own data bank,

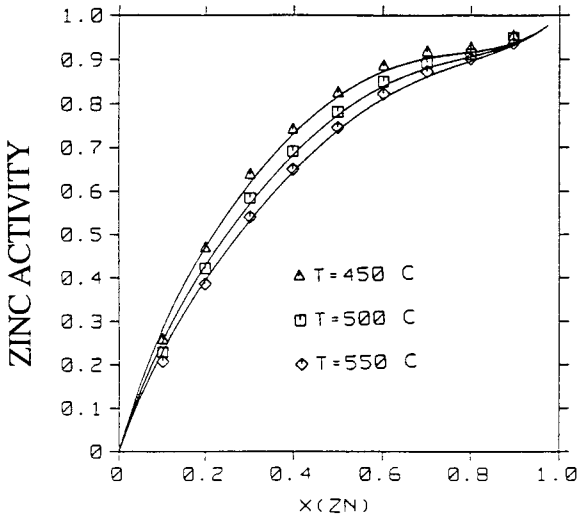

Fig. 16. The zinc-activity measurement of Fiorani and Oleari [10] in the isoplethic cut $x_{Sn}=3$ x_{Pb} are in excellent agreement with our modelisation: three calculated curves at 450, 500 and 550°C.

after the optimisation of all the data. With this, it is very easy to calculate any information concerning the provision of the process.

Appendix

References relating to figures only

1. J. Lumsden, Disc. Farad. Soc. 4 (1948) 60
2. O.J. Kleppa, J. Amer. Chem. Soc. 74 (1952) 6052
3. Z. Moser, L. Zabdyr, W. Gasior, J. Salawa, W. Zakulski, J. Phase Equilibria. 15 (1994) 643
4. F.D. Rosenthal, G.J. Mills, F.J. Dunkerley, Metall. Trans. AIME. 212 (1958) 153
5. J.D. Esdaile, F. Swett, Metall. Trans. AIME. 14A (1983) 2211
6. R. Hultgren, S.A. Lever, Metall. Trans. AIME. 185 (1949) 67
7. O.J. Kleppa, J. Phys. Chem. 59 (1955) 175
8. M. Azzaoui, Thèse, Université Henri Poincaré Nancy I, 19 juin 1993
9. R. Hultgren, P.D. Desai, D.T. Hawkins, M. Gleiser, K.K. Kelley, D.D. Wagman, Selected Values of the Thermodynamic Properties of Alloys American Society for Metals, Metals Park, Ohio, 1973

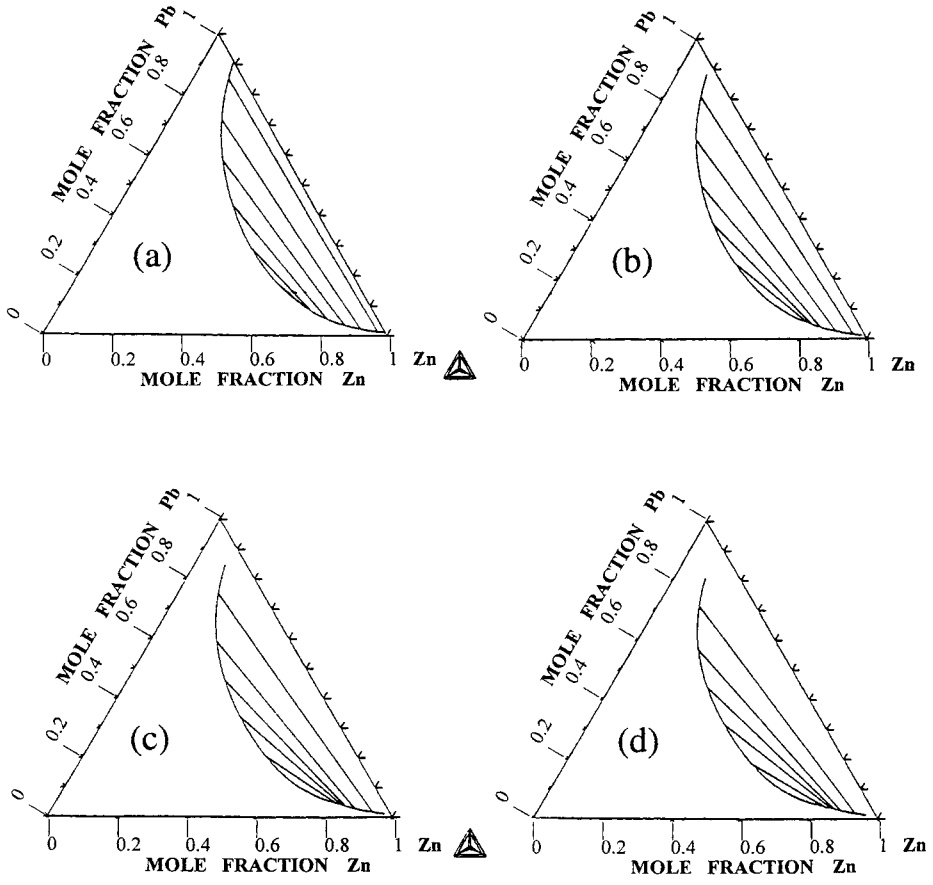

Fig. 17. To represent the quaternary miscibility gap in the (M, Pb, Sn, Zn) system together with the tie-lines in a two-dimensional plot, it is easy to fix the temperature and the M-activity. This representation looks very similar to a ternary isothermal section. Here at 480°C four different values of the M-activity from 10^{-10} to 10^{-1}. Note that the miscibility gap does not join the binary (Pb, Zn) border.

10. J.F. Trahan, L.L. Lacy, Mat. Sc. Eng. 33 (1978) 249
11. Z. Moser, W. Gasior, Bull. Pol. Acad. Sci. 31 (1983) 19
12. O.J. Kleppa, J. Phys. Chem. 59 (1955) 354
13. M. Fiorani, V. Valenti, Gazz. Chim. Ital. 85 (1955) 607

References

[1] T.B. Massalski, H. Okamoto, P.R. Subramanian, L. Kacprzak, Binary Alloys Phase Diagrams, 2nd edn., vols. 1, 2, 3, A.S.M., International, Materials Park, OH, 1990.
[2] A. Dinsdale, CALPHAD 15 (1991) 317.
[3] B. Sundman, B. Jansson, J.O. Anderson, CALPHAD 9 (1985) 153.
[4] O. Redlich, A.T. Kister, Ind. Eng. Chem. 40 (1948) 345.
[5] M. Hillert, CALPHAD 4 (1980) 1.
[6] A. Bourkba, J.M. Fiorani, C. Naguet, J. Hertz, Z. Metallkd. 87 (1996) 773.
[7] C. Naguet, J.M. Fiorani, A. Bourkba, J. Hertz, Z. Metallkd. 88 (1997) 469.
[8] A. Bourkba, Thèse de Doctorat ès Sciences Physiques, Université IBNOU ZOHR, AGADIR (Maroc) 29 octobre 1996.
[9] D.D. Todd, W.A. Oates, Metall. Trans. AIME 230 (1964) 244–246.
[10] M. Fiorani, L. Oleari, Ricerca Scientifica 29 (1959) 2349.
[11] M. Srivastava, R.C. Sharma, J. Phase Equilibria. 14 (1993) 700.
[12] N.I. Chourov, Physical Sciences Thesis, Svredlovsk University, Russia, 1974.